

INTENSITY-BASED POINT-SPREAD-FUNCTION-AWARE REGISTRATION FOR MULTI-VIEW APPLICATIONS IN OPTICAL MICROSCOPY

Nikhil Chacko¹, Kevin G. Chan¹, Michael Liebling^{1,2}

¹Electrical and Computer Engineering, University of California, Santa Barbara, CA 93106, U.S.A.

²Idiap Research Institute, CH-1920 Martigny, Switzerland

ABSTRACT

We present an algorithm to spatially register two volumetric datasets related via a rigid-body transform and degraded by an anisotropic point-spread-function (PSF). Registration is necessary, for example, when fusing data in multi-view microscopy. Automatic algorithms that only rely on maximizing pixel similarity, without accounting for the anisotropic image formation process, provide poor results in such applications. We propose to solve this problem by re-blurring the reference and test data with transformed forms of the PSF, in order to make them comparable, before minimizing the mean squared intensity difference between them. Our approach extends the pyramid-based sub-pixel registration algorithm proposed by Thévenaz et al., 1998, that employs an improved form of the Marquardt-Levenberg algorithm. We show, via simulations, that our method is more accurate than the conventional approach that does not account for the PSF. We demonstrate our algorithm in practice by registering multi-view volumes of a zebrafish larva acquired using a wide-field microscope.

Index Terms— Multi-view, registration, point-spread-function, Marquardt-Levenberg, pyramid, optical microscopy.

1. INTRODUCTION

Optical microscopy offers the unique possibility of imaging living samples under conditions akin to their native state. However, the technique often suffers from anisotropic resolution owing to the image formation process, which consists of a 3D convolution operation with the imaging system's (anisotropic) point-spread-function (PSF) [1]. Despite recent advances to design instruments that exhibit nearly isotropic PSFs, many commonly used microscopes have a PSF that is more elongated in the axial direction, with wide-field microscopy having the most severe form of anisotropy, and techniques such as confocal, two-photon, and light-sheet microscopy having the least. This anisotropy translates to an axial resolution that is worse than the lateral resolution in the acquired data. Multi-view microscopy attempts to circumvent this problem by merging acquisitions from multiple tilted directions [1–7]. However, operations therein, such as multi-view fusion and deconvolution, require the volumes to be precisely registered before they can be used.

Several approaches have been proposed to address this registration problem. Heintzmann *et al.* [3] presented a mostly *manual* registration algorithm that relies on an interactive selection of salient points in the input volumes, which are used as an alignment aid. However, such a manual technique tends to be both laborious and inaccurate. A second class of algorithms that can be considered *automatic* relies on fiducial markers, such as fluorescent beads, added in moderate concentration to the prepared sample [8, 9], which are subsequently detected and used for registration. Although these approaches were shown to be accurate, they require a special method of sample preparation. Moreover, the markers added can interfere with the visibility of the sample being imaged. To alleviate this problem, Krzic *et al.* [6] designed an imaging system where such fiducial markers are only used for hardware calibration, thereby averting the need to add beads along with the sample during imaging. In lieu of external markers, Keller *et al.* [10] followed a data-specific strategy to automatically detect cell nuclei and treat them as landmarks for multi-view registration. Others have used techniques such as cross-correlation [1, 2, 4, 5] based on the pixel-wise similarity between datasets for registration. However, such approaches can lead to inaccuracies because they ignore the anisotropy inherent in the image formation process. A simple example is detailed in Fig. 1, where a sample (Fig. 1(a-c)) is convolved with an anisotropic PSF. The convolution shifts the optical center of mass (and other moments) in directions within the object coordinates [11] (Fig. 1(d-f)), leading conventional pixel-based matching methods (which would also match the center of mass) to yield a biased solution.

In this paper, we propose to modify the registration cost function by *cross-blurring* the reference and test datasets (Fig. 1(d-f)) using PSFs tilted by the candidate transformation, so that the image volumes are comparable and identically degraded at convergence (Fig. 1(g-i)). We demonstrate our approach using both simulations and experimental data.

The paper is organized as follows. In Section 2, we describe our notations, the cost function that we wish to minimize, and our optimization strategy. In Section 3, we illustrate the applicability of our method on simulated and experimental datasets, and finally conclude in Section 4.

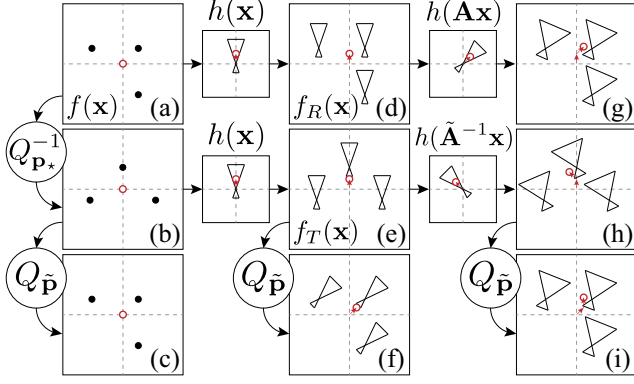


Fig. 1: An illustration on how PSF affects data registration. The red circle denotes the center of mass in each case. (a-c) Registration of datasets uncorrupted by PSF. (d-f) Reference, test, and registered test, respectively. (g-i) *Cross-blurred* forms of the datasets in (d-f). Note that the center of mass coincides in (g) and (i), unlike that in (d) and (f).

2. METHOD

2.1. Problem Formulation

We consider a function $f(\mathbf{x})$, $\mathbf{x} \in \mathbb{R}^3$, that represents an object being imaged. We assume f undergoes a geometric transformation that can be parameterized by (i) a rotation matrix, \mathbf{A} , of size 3×3 , and (ii) a translation vector, \mathbf{b} , of size 3×1 . We represent this using (i) a rotation operator, $R_{\mathbf{A}}$, and (ii) a translation operator, $T_{\mathbf{b}}$, defined as follows:

$$R_{\mathbf{A}} \{f\}(\mathbf{x}) \triangleq f(\mathbf{A}\mathbf{x}) \quad (1)$$

$$T_{\mathbf{b}} \{f\}(\mathbf{x}) \triangleq f(\mathbf{x} + \mathbf{b}). \quad (2)$$

We jointly express the parameters \mathbf{A} and \mathbf{b} as \mathbf{p} . We represent the sequence of transformations parameterized by \mathbf{p} as:

$$Q_{\mathbf{p}} \{f\}(\mathbf{x}) \triangleq (R_{\mathbf{A}} \circ T_{\mathbf{b}} \circ f)(\mathbf{x}) \quad (3)$$

$$= f(\mathbf{A}\mathbf{x} + \mathbf{b}), \quad (4)$$

$$Q_{\mathbf{p}}^{-1} \{f\}(\mathbf{x}) \triangleq (T_{-\mathbf{b}} \circ R_{\mathbf{A}^{-1}} \circ f)(\mathbf{x}) \quad (5)$$

$$= f(\mathbf{A}^{-1}(\mathbf{x} - \mathbf{b})). \quad (6)$$

In particular, we consider two volumes—the reference f_R and the test f_T (which is to be geometrically transformed to match f_R)—defined as follows:

$$f_R(\mathbf{x}) \triangleq (f * h)(\mathbf{x}), \quad (7)$$

$$f_T(\mathbf{x}) \triangleq (Q_{\mathbf{p}_*}^{-1} \{f\} * h)(\mathbf{x}). \quad (8)$$

Specifically, \mathbf{p}_* represents the unknown set of parameters (\mathbf{A}_* and \mathbf{b}_*) that we wish to estimate and that characterize the geometrical transformation undergone by the object f between the acquisitions of f_R and f_T .

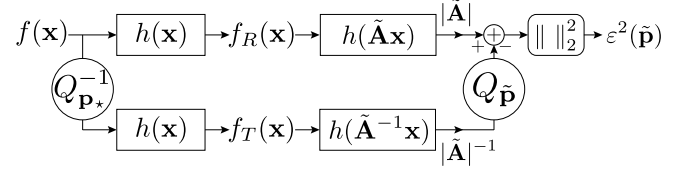


Fig. 2: The proposed cost function ε^2 to be minimized using *cross-blurred* forms of the reference f_R and test f_T datasets.

2.2. Proposed Registration Approach

The motivation of our approach stems from the fact that even if the correct geometrical transform $Q_{\mathbf{p}_*}$ is applied to the test data f_T , the resulting volume $Q_{\mathbf{p}_*} \{f_T\}$ will be different from the reference f_R . This is because the geometrical transform $Q_{\mathbf{p}_*}$ also applies to the convolution kernel h , thus making an intensity-based similarity criterion unsuitable (Fig. 1(d-f)). To overcome this problem, we propose to *cross-blur* the reference and test data with each other's effective PSF before using any candidate transform $Q_{\tilde{\mathbf{p}}}$ (Fig. 1(g-i)).

Using Eq. (7) in conjunction with properties of convolution operations, the convolution between f_R and a rotated version of h can be expressed as:

$$(f_R * R_{\mathbf{A}_*} \{h\})(\mathbf{x}) = (f * h * R_{\mathbf{A}_*} \{h\})(\mathbf{x}). \quad (9)$$

Similarly, using Eq. (8) and properties of affine transforms [12], applying $Q_{\tilde{\mathbf{p}}}$ after subjecting f_T to a convolution with an inverse-rotated form of h is equivalent to the following:

$$Q_{\tilde{\mathbf{p}}} \{f_T * R_{\tilde{\mathbf{A}}^{-1}} \{h\}\}(\mathbf{x}) = |\tilde{\mathbf{A}}| (Q_{\tilde{\mathbf{p}}} \{f_T\} * h)(\mathbf{x}) \quad (10)$$

$$= |\tilde{\mathbf{A}}|^2 (f * R_{\tilde{\mathbf{A}}_*} \{h\} * h)(\mathbf{x}), \quad (11)$$

where $|\tilde{\mathbf{A}}|$ denotes the determinant of the matrix $\tilde{\mathbf{A}}$. For the correct transform, since the *cross-blurred* volumes are equivalent except for a scaling constant (compare Eqs. (9) and (11)), we can estimate the optimal set of parameters \mathbf{p}_* via the following cost function (see also Fig. 2):

$$\varepsilon^2(\tilde{\mathbf{p}}) \triangleq \left\| |\tilde{\mathbf{A}}| (f_R * R_{\tilde{\mathbf{A}}} \{h\})(\mathbf{x}) - |\tilde{\mathbf{A}}|^{-1} Q_{\tilde{\mathbf{p}}} \{f_T * R_{\tilde{\mathbf{A}}^{-1}} \{h\}\}(\mathbf{x}) \right\|_2^2 \quad (12)$$

$$= \left\| |\tilde{\mathbf{A}}| (f_R * R_{\tilde{\mathbf{A}}} \{h\})(\mathbf{x}) - (Q_{\tilde{\mathbf{p}}} \{f_T\} * h)(\mathbf{x}) \right\|_2^2, \quad (13)$$

where $\tilde{\mathbf{p}}$ comprises $\tilde{\mathbf{A}}$ and $\tilde{\mathbf{b}}$. Since $|\tilde{\mathbf{A}}| = 1$ when $\tilde{\mathbf{A}}$ is a rotation matrix, we can ignore this scaling constant for all purposes in this paper.

To estimate the optimal set of parameters \mathbf{p}_* , we solve a variant of $\partial \varepsilon^2(\tilde{\mathbf{p}}) / \partial \tilde{\mathbf{p}} = 0$ with an improved form of the

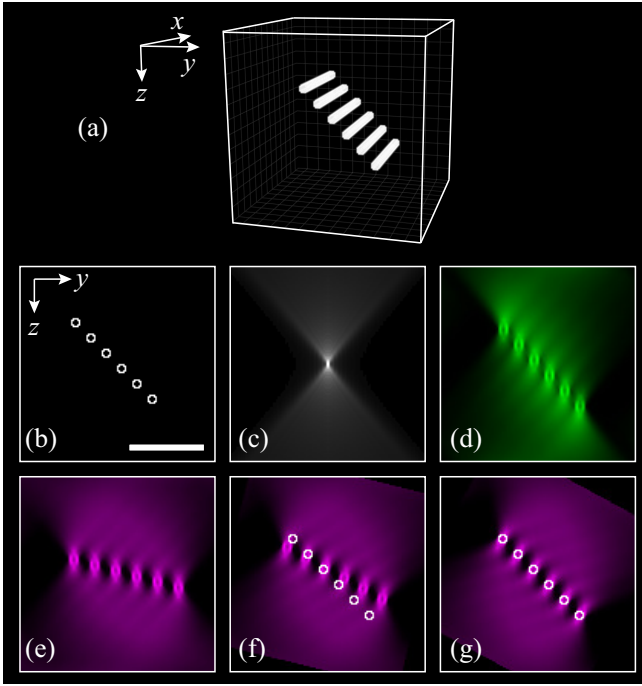


Fig. 3: (a) 3D perspective of the object used in simulations. (b-g) Maximum intensity projection (MIP) in the yz plane of f , h (after gamma-correction of $\gamma = 0.3$), f_R , f_T , the registered results using the traditional, and our proposed approach, respectively. For comparison, (b) has been overlaid on the registered results shown in (f) and (g). Scale bar is $25\mu m$.

Marquardt-Levenberg (ML) algorithm [13] using an approach similar to that proposed by Thévenaz *et al.* [14]. As in the original algorithm, we employ a multi-resolution approach by using a dyadic pyramid based on cubic B-splines to represent the volumes at multiple scales. Following a coarse-to-fine strategy, the algorithm first achieves a quick registration based on the large-scale features in the data, and subsequently makes changes for progressively finer details. This is advantageous with respect to both computation time and robustness against local minima, especially since computations (and convolutions during re-blurring) are in 3D. We consider the routine to have converged at each scale when the total relative change in the parameters has dropped below a set threshold.

3. EXPERIMENTS

3.1. Validation with simulated data

For validation purposes, we considered a synthetic dataset consisting of six parallel hollow bars [15] (Fig. 3(a-b)) as our uncorrupted volume, f . We then used a software package [16] to generate a Gibson & Lanni 3D PSF model (Fig. 3(c)), h , applicable for wide-field microscopes, with the following parameters: immersion refractive index = 1 (air), sample refractive index = 1.33, numerical aperture (NA) = 0.7, working

distance = 2 mm, particle position = $0\mu m$, sampling step $\Delta x = \Delta y = \Delta z = 0.5\mu m$, excitation wavelength = 495 nm, and emission wavelength = 509 nm. Using f and h , we generated the reference f_R (Fig. 3(d)). Next, we rotated f by an angle of 30° about the x -axis, and translated it by a vector $[b_0, b_1, b_2]^\top$, where b_0 , b_1 , and b_2 were chosen from a uniform distribution between 0 and 5, and finally convolved it with h to form f_T (Fig. 3(e)). With an initial guess equal to the identity transformation, we then attempted to estimate \mathbf{p}_* using two different approaches: (i) using the PSF ignorant form of the improved ML algorithm [14] (*i.e.* assuming $h(\mathbf{x}) = \delta(\mathbf{x})$), and (ii) using our proposed algorithm. The simulation was run over 10 random instances, and the mean error in the estimated angle was found to be 11.55° using the traditional approach, and 1.71° using our proposed algorithm. Examples of the registered results obtained using the two algorithms are shown in Fig. 3(f) and (g), respectively. We repeated this experiment by also using a Gaussian approximation of the PSF corresponding to a disk scanning confocal microscope [17] with NA = 0.3, pinhole radius = 5 Airy units, and similar parameters as before. For this case, the mean error in the estimated angle was recorded as 5.69° using the traditional approach, and 0.39° using our proposed algorithm.

3.2. Illustration on experimentally acquired data

To prove the applicability of our approach for experimental datasets, we used an inverted wide-field microscope equipped with a $10\times/0.3$ dry objective to acquire 3D volumes of a 25-hpf (hours post-fertilization)-old transgenic zebrafish larva (*Tg(fli1a:EGFP)*), which expresses green fluorescent protein in the vasculature. We inserted the larva in a tube made from fluorinated ethylene propylene (FEP), whose refractive index is close to that of water, and rotated the tube using a stepper motor for six multi-view acquisitions (Fig. 4(d)). Treating the first volume as the reference, we recursively registered each subsequent dataset to its aligned predecessor. The registered form of the final volume is shown together with the first reference in Fig. 4(a-c). The results demonstrate that despite the anisotropic resolution, characteristic of wide-field microscopy, our approach correctly matches the curvature and bright features of the vasculature, without erroneously matching the dominant blur (see also supplemental movie).

4. CONCLUSION

We have derived an automatic intensity-based registration routine and have demonstrated its suitability for aligning volumes that were acquired using imaging systems with severely anisotropic point spread functions. The simulation results, which showed an accuracy of around an order of magnitude over the traditional scheme, demonstrates the benefits of such an approach that integrates the imaging model. The good alignment we observed using multi-view volumes from a

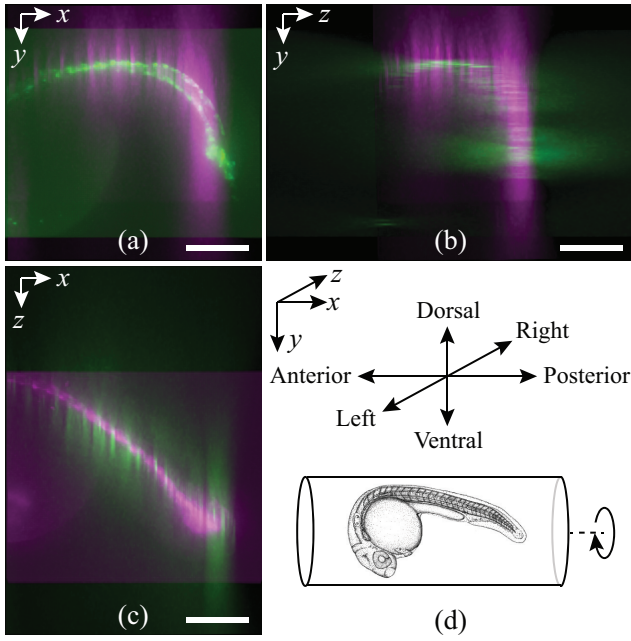


Fig. 4: (a-c) MIP of the first volume (green) and the recursively registered final volume (magenta) (originally acquired after a rotation of approximately 90° about the x -axis) in the xy , yz , and xz planes, respectively. (d) A schematic representation showing the relative position of the sample and the axis of rotation in our experimental setup. Scale bar is $200\mu\text{m}$.

wide-field microscope, whose PSF anisotropy is particularly strong, confirms our method's potential for applications in multi-view microscopy.

5. REFERENCES

- [1] P. J. Shaw, D. A. Agard, Y. Hiraoka, and J. W. Sedat, "Tilted view reconstruction in optical microscopy. Three-dimensional reconstruction of *Drosophila melanogaster* embryo nuclei," *Biophysical J.*, vol. 55, no. 1, pp. 101–110, 1989.
- [2] C. J. Cogswell, K. G. Larkin, and H. U. Klemm, "Fluorescence microtomography: multiangle image acquisition and 3D digital reconstruction," in *Electr. Imag.*, 1996, pp. 109–115.
- [3] R. Heintzmann, G. Kreth, and C. Cremer, "Reconstruction of axial tomographic high resolution data from confocal fluorescence microscopy: a method for improving 3D fish images," *Analytical Cellular Pathology*, vol. 20, no. 1, pp. 7–15, 2000.
- [4] R. Heintzmann and C. Cremer, "Axial tomographic confocal fluorescence microscopy," *J. of Microscopy*, vol. 206, no. 1, pp. 7–23, 2002.
- [5] J. Swoger, P. Verveer, K. Greger, J. Huisken, and E. H. K. Stelzer, "Multi-view image fusion improves resolution in three-dimensional microscopy," *Opt. Express*, vol. 15, no. 13, pp. 8029–8042, Jun. 2007.
- [6] U. Krzic, S. Gunther, T. E. Saunders, S. J. Streichan, and L. Hufnagel, "Multiview light-sheet microscope for rapid *in toto* imaging," *Nature Methods*, vol. 9, no. 7, pp. 730–733, 2012.
- [7] N. Chacko and M. Liebling, "Fast thresholded multi-channel Landweber algorithm for wavelet-regularized multi-angle deconvolution," in *Proc. SPIE*, 2013, pp. 885819 1–10.
- [8] S. Preibisch, S. Saalfeld, J. Schindelin, and P. Tomancak, "Software for bead-based registration of selective plane illumination microscopy data," *Nature Methods*, vol. 7, no. 6, pp. 418–419, 2010.
- [9] M. Temerinac-Ott, M. Keuper, and H. Burkhardt, "Evaluation of a new point clouds registration method based on group averaging features," in *20th Int. Conf. on Pattern Recognition (ICPR)*, Aug. 2010, pp. 2452–2455.
- [10] P. J. Keller, A. D. Schmidt, J. Wittbrodt, and E. H. K. Stelzer, "Reconstruction of zebrafish early embryonic development by scanned light sheet microscopy," *Science*, vol. 322, no. 5904, pp. 1065–1069, 2008.
- [11] C. A. Laury-Micoulaut, "The n -th centered moment of a multiple convolution and its applications to an intercloud gas model," *Astronomy and Astrophysics*, vol. 51, pp. 343–346, 1976.
- [12] R. N. Bracewell, K. Y. Chang, A. K. Jha, and Y. H. Wang, "Affine theorem for two-dimensional Fourier transform," *Electronics Lett.*, vol. 29, no. 3, 1993.
- [13] D. W. Marquardt, "An algorithm for least-squares estimation of nonlinear parameters," *SIAM J. on App. Math.*, vol. 11, no. 2, pp. 431–441, 1963.
- [14] P. Thévenaz, U. E. Ruttimann, and M. Unser, "A pyramid approach to subpixel registration based on intensity," *IEEE Trans. on Image Proc.*, vol. 7, no. 1, pp. 27–41, Jan. 1998.
- [15] <http://bigwww.epfl.ch/deconvolution/?p=bars>.
- [16] H. Kirshner, F. Aguet, D. Sage, and M. Unser, "3-D PSF fitting for fluorescence microscopy: Implementation and localization application," *J. of Microscopy*, vol. 249, no. 1, pp. 13–25, Jan. 2013.
- [17] B. Zhang, J. Zerubia, and J.-C. Olivo-Marin, "Gaussian approximations of fluorescence microscope point-spread function models," *Appl. Opt.*, vol. 46, no. 10, pp. 1819–1829, Apr 2007.